Dissolution Rates of Upper Mantle Minerals in an Alkali Basalt Melt at High Pressure: An Experimental Study and Implications for Ultramafic Xenolith Survival

Article *in* Journal of Petrology · October 1986

DOI: 10.1093/petrology/27.5.1157

2 authors, including:

Mark Brearley
Chevron
21 PUBLICATIONS **626** CITATIONS

Dissolution Rates of Upper Mantle Minerals in an Alkali Basalt Melt at High Pressure: An Experimental Study and Implications for Ultramafic Xenolith Survival

by MARK BREARLEY* AND CHRISTOPHER M. SCARFE

Experimental Petrology Laboratory, Department of Geology, University of Alberta, Edmonton, Alberta, Canada T6G 2E3

(*Received 12 November 1985; revised typescript accepted 7 April 1986*)

ABSTRACT

The dissolution rates of the major upper mantle minerals olivine, orthopyroxene, clinopyroxene, spinel, and garnet have been determined in an alkali basalt melt at superliquidus temperatures and 5, 12, and 30 kb. At low pressure where olivine is the liquidus phase of the basalt, olivine has a slower dissolution rate than clinopyroxene; however, at higher pressure where clinopyroxene is the liquidus phase, clinopyroxene has a slower dissolution rate than olivine. The relative rates of dissolution of olivine and clinopyroxene at each pressure are, therefore, governed by their relative stabilities in the melt and hence by the structure of the melt. As the degree of superheating above the liquidus increases at each pressure, the dissolution rates of olivine and clinopyroxene converge, suggesting that the melt undergoes temperature-induced structural changes.

Orthopyroxene has a dissolution rate similar to olivine at high pressure and similar to clinopyroxene at low pressure. Spinel has the slowest dissolution rate at each pressure. Garnet dissolves very rapidly at 12 kb and at a comparable rate of olivine at 30 kb. The dissolution rates determined in the experiments vary from $9{\cdot}21 \times 10^{-9}$ cm s^{-1} for spinel at 5 kbar and 1250 °C to $3{\cdot}83 \times 10^{-5}$ cm s^{-1} for garnet at 30 kb and 1500 °C.

Textures produced during the dissolution experiments are related to mineral stability in the melt at each pressure and are independent of the degree of superheating. The mineral phases that are stable on or near the liquidus exhibit no reaction; whereas complex reaction textures and crystallization characterize dissolution of minerals that are relatively unstable in the melt.

Concentration profiles in the melt adjacent to the same crystal for different experimental durations are identical, indicating that dissolution is time-independent and a steady-state process. However, cation diffusion coefficients calculated for single-component oxides in the melt reveal that dissolution may not be completely controlled by diffusion of cations away from the crystal/melt interface. The apparent diffusivities positively correlate with the dissolution rate, which suggests that the stability of the mineral is an important factor to consider when deriving diffusion coefficients from these experiments. Other factors that may be involved are multi-component effects and the nature of the diffusing species in the melt.

A simple model has been constructed that predicts the survival of ultramafic xenoliths in alkali basalt magmas as a function of xenolith radius, magma ascent time and superheating. The results of the model suggest that the relative proportions of peridotite and pyroxenite xenoliths brought to the surface in alkali basalts are generally representative of their proportions as constituents of the upper mantle. Further experiments using different melt compositions are required to extend the model.

* Present address: Institute of Geophysics and Planetary Physics, University of California, Los Angeles, California 90024.

[*Journal of Petrology*, Vol. 27, Part 5, pp. 1157–1182]

INTRODUCTION

The predominance of peridotite xenoliths found in alkali basalts and kimberlites is evidence for an upper mantle composed of olivine-rich peridotite (e.g., Yoder, 1976). Nevertheless, pyroxene-rich xenoliths are well represented at a few localities. The eclogites at the Roberts Victor Mine, South Africa (Carswell & Dawson, 1970; Dawson, 1980, 1981) and the abundant garnet pyroxenites on Hawaii (Jackson & Wright, 1970) are two examples. The general paucity of pyroxenites and eclogites relative to peridotite xenoliths has led to the suggestion that either: (1) pyroxenites are only locally important constituents of the upper mantle (Yoder, 1976); or (2) they preferentially dissolve in alkalic magmas while in the upper mantle or during transport to the surface (Kutolin & Agafonov, 1978).

The dissolution of crystals in silicate melts has been studied by a number of workers (e.g., Cooper & Kingery, 1964; Cooper & Schut, 1980; Scarfe *et al.*, 1980; Harrison & Watson, 1983, 1984; Donaldson, 1984, 1985; Kuo & Kirkpatrick, 1985; Thornber & Huebner, 1985; Tsuchiyama 1985, 1986*a*; Chekhmir & Epel'baum, 1986). The theoretical aspects of crystal dissolutions in melts have been treated in detail by Cooper & Kingery (1964), Kuo & Kirkpatrick (1985) and Tsuchiyama (1986*b*).

However, few studies have dealt with the dissolution rates of mafic minerals in mafic melts (Kutolin & Agafonov, 1978; Scarfe *et al.*, 1980; Donaldson, 1984, 1985; Thornber & Huebner, 1985). Kutolin & Agafonov (1978) performed experiments at 1 b to determine the relative dissolution rates of the major upper mantle minerals in an alkalic melt. They concluded that pyroxene dissolves more rapidly than olivine. This behavior was also observed by Scarfe *et al.* (1980) at high pressure (12·5–20 kb).

Because of the absence of systematic data on the dissolution rates of ultramafic xenoliths in alkali basalt melts at high pressure, we have investigated the dissolution rates of the major upper mantle minerals olivine, orthopyroxene, clinopyroxene, garnet, and spinel in an alkali basalt melt to pressures of 30 kb. We show that the relative rates of dissolution of these minerals at each pressure is strongly related to the liquidus phase relationships of the melt. It is concluded that dissolution is a steady-state process and that cation diffusivities in this multi-component system are dependent on several factors including the dissolution rate of the mineral. By utilizing these data, we present a simple model that predicts the dissolution of ultramafic xenoliths in alkali basalt magmas and we briefly discuss the petrological significance of the conclusions.

EXPERIMENTAL PROCEDURE

Dissolution experiments

Starting materials for the dissolution experiments were an alkali basalt rock powder and crystals of olivine, orthopyroxene, chrome diopside, spinel and garnet, separated from ultramafic xenoliths or megacrysts (Table 1). The alkali basalt, although apparently somewhat evolved, was chosen because it is reasonably representative of the composition of basalts associated with ultramafic xenoliths in British Columbia (Fujii & Scarfe, 1982; Nicholls *et al.*, 1982; Brearley *et al.*, 1984). The crystals were ground into spheres using a method described by Bond (1951). Each sphere was cleaned ultrasonically in dilute HCl, washed in distilled water, dried, and then measured at least six times with a micrometer. The basalt was initially dried at 900 °C for 24 h at the QFM oxygen buffer, and stored at 110 °C between experiments. The spheres were placed on a thin bed of alkali basalt powder in a graphite capsule, which was then packed tightly with more powder. The graphite capsule was fired at 800 °C for approximately 3 min both before and after the capsule was loaded to drive off any water adsorbed on the surface. The capsule was then inserted into a talc–pyrex

TABLE 1

Starting materials for dissolution experiments

	1	*2*	*3*	*4*	*5*	*6*
SiO_2	40·0	n.d.	42·31	54·7	52·3	48·6
TiO_2	n.d.	0·24	0·81	n.d.	0·41	2·20
Al_2O_3	n.d.	64·7	21·68	4·54	6·47	15·6
Fe_2O_3	n.a.	4·30	n.a.	n.a.	n.a.	3·13
FeO	10·0	7·73	10·44	5·97	2·67	8·53
MnO	0·15	0·12	0·38	0·15	n.d.	0·16
MgO	48·2	22·2	19·40	34·3	16·2	6·30
CaO	0·18	n.d.	4·75	0·72	19·7	9·85
Na_2O	n.d.	n.d.	0·12	n.d.	1·45	3·50
K_2O	n.d.	n.d.	n.d.	n.d.	n.d.	1·21
NiO	0·48	0·56	n.d.	0·15	0·05	n.d.
Cr_2O_3	n.d.	n.d.	0·46	0·49	1·19	n.d.
P_2O_5	n.d.	n.d.	n.d.	n.d.	n.d.	0·51
H_2O	n.a.	n.a.	n.a.	n.a.	n.a.	0·02
Total	99·01	99·85	100·35	101·02	100·44	99·61

(1) olivine, (2) spinel, (3) garnet, (4) orthopyroxene, (5) clinopyroxene (all from Summit Lake, British Columbia, Brearley *et al.*, 1984), (6) KR-13 alkali basalt (from West Kettle River, British Columbia, Fujii & Scarfe, 1982). FeO in alkali basalt by wet chemistry, Fe_2O_3 in spinel by stoichiometry. All analyses by energy dispersive microprobe methods described in text. Basalt analysis performed on a bead, fused at 1300 °C at the QFM oxygen buffer. n.d.—not detected, n.a.—not analyzed.

piston-cylinder assembly and dried for 8 h at 110 °C. Graphite capsules were used in all experiments in order to maintain the oxygen fugacity in the wustite stability field (Thompson & Kushiro, 1972).

Experiments were performed in a solid-media piston-cylinder apparatus (Boyd & England, 1960). Temperatures were monitored by a Pt/Pt 13 per cent Rh thermocouple without any correction for pressure and are accurate to ± 10 °C. Pressures were monitored continuously during each run with an Heise gauge and are accurate to $\pm 0{\cdot}5$ kb. For further details of the calibration and experimental procedures see Fujii & Scarfe (1985). Time series experiments were done for each mineral in order to evaluate the time-dependence of dissolution. All runs were quenched at a rate of approximately 125 °C s^{-1} by switching off the power to the graphite furnace. At the termination of each experiment, the graphite capsule was sectioned and ground until the maximum diameter of the partially dissolved spheres was exposed.

In order to detect any possible incorporation of water in the melt during the experiment, wafers of glass from a one hour experiment were analyzed for H_2O by a micromanometric technique (Harris, 1981). The concentration of water was $< 0{\cdot}1$ wt. per cent, which is not considered sufficient to affect the rate of dissolution (e.g., Harrison & Watson, 1983).

Phase equilibrium experiments

The liquidus phases of KR-13 alkali basalt were determined from 5 to 30 kb pressure in the piston-cylinder apparatus. Graphite capsules were loaded with alkali basalt powder in the same manner as described in the previous section. Experiments were run up to the desired temperature and were held at that temperature for a duration of 1 day, before quenching. Run

products were identified optically and the crystalline phases were examined with an electron microprobe for major elements. The principal objective of the liquidus phase equilibrium experiments was to determine the liquidus phase and the approximate temperatures of the liquidus at each pressure. Therefore, no reversal experiments were attempted.

ANALYTICAL METHOD

Concentration profiles in the mineral spheres and in the glass next to the mineral spheres in the dissolution experiments, and analyses of the crystalline phases in the liquidus phase equilibrium experiments were obtained by both energy and wavelength dispersive microprobe methods. Excellent agreement was found between the EDA and WDA analyses when both methods were used on the same material. The agreement between EDA and WDA analyses has been previously noted by Fujii & Scarfe (1985). For EDA, a 15 kV accelerating potential, 4 nA probe current and 240 s counting time were employed. For WDA, a 10 nA probe current and 40 s counting times were used on peak and background positions. A point beam was used in both EDA and WDA analysis. All microprobe data were processed with full ZAF corrections using EDATA2 (Smith & Gold, 1979). No significant secondary fluorescence effects were found at the crystal/glass interface during energy dispersive analysis of a blank olivine–basalt couple.

RESULTS OF EXPERIMENTS

Liquidus phase equilibria

The results of the liquidus phase equilibria experiments are shown in Fig. 1. The liquidus phase at 5 kb is olivine of Fo_{75} composition. From approximately 7·5 to at least 30 kb

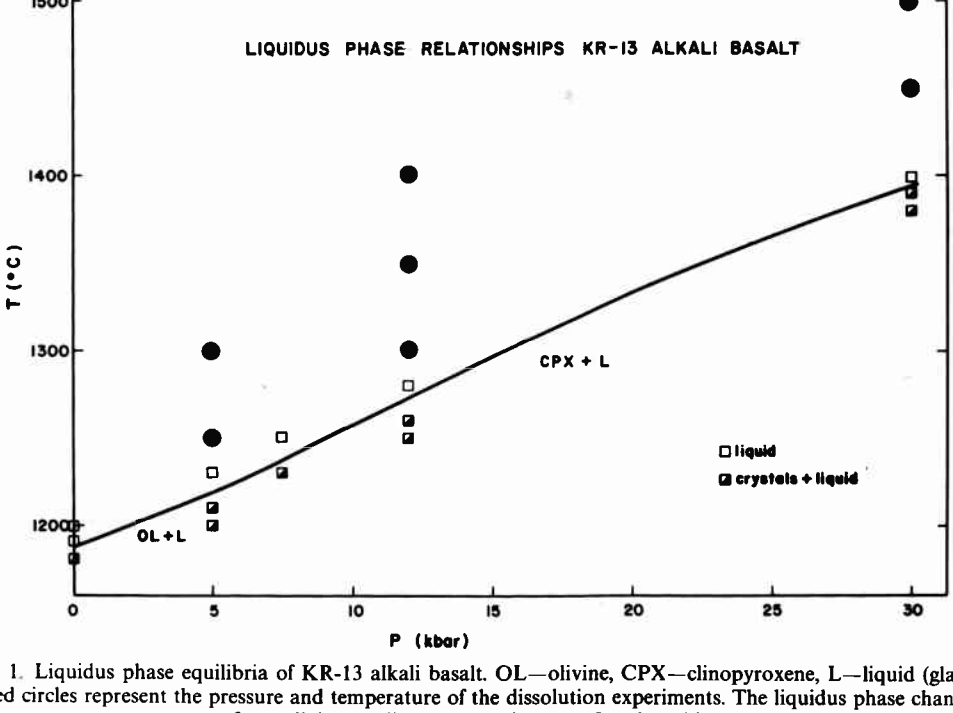

IG. 1. Liquidus phase equilibria of KR-13 alkali basalt. OL—olivine, CPX—clinopyroxene, L—liquid (glass). illed circles represent the pressure and temperature of the dissolution experiments. The liquidus phase changes from olivine to clinopyroxene between 5 and 7·5 kb.

Crystal/melt textur

The textures pro

Textures at 5 kb

dissolution of orth
crystal/melt interf
crystallize (Fig. 2a
Clinopyroxene als
(Fig. 2b). Thereaft
forms a vermicular
original spinel com
crystals (Fig. 2c).

Textures at 12 k

Spinel has a simi
relationship. Initia
Further dissolution
spinel (Fig. 2d). Th

Textures at 30 k

extures character
pyroxene with int
represents the dif

Olivine
Orthopyroxene
Clinopyroxene
Spinel
Garnet

---

x = mole fraction
chromite
xenocryst

clinopyroxene (augite) is the liquidus phase. In accord with previous studies, the Na_2O and Al_2O_3 content of the clinopyroxene increase with increasing pressure (e.g., Green & Ringwood, 1968; Bultitude & Green, 1971). At 30 kb, the Al_2O_3 content is 14·5 wt. per cent. The liquidus temperatures, bracketed to ± 10 °C, were used to determine the temperatures at which the dissolution experiments were conducted.

Dissolution experiments

Crystal/melt textural relationships

The textures produced during the dissolution experiments are summarized in Table 2.

Textures at 5 kb. In all experiments at 5 kb, olivine crystals have no reaction texture. The dissolution of orthopyroxene produces a thin band of equant chromite crystals at the original crystal/melt interface and further dissolution causes olivine crystals of Fo_{90} composition to crystallize (Fig. 2a). Melt (glass) forms intersertal patches between the olivine crystals. Clinopyroxene also reacts to form a thin layer of chromite crystals at the original interface (Fig. 2b). Thereafter, dissolution of clinopyroxene produces glass only. Spinel dissolution forms a vermicular rim of spinels more Cr- and Fe-rich and less Mg- and Al-rich than the original spinel composition. Irregular patches of glass are trapped between the vermicular crystals (Fig. 2c).

Textures at 12 kb. Olivine, orthopyroxene, and clinopyroxene exhibit no reaction textures. Spinel has a similar vermicular texture to that at 5 kb. Garnet has a complex reaction relationship. Initially, dissolution of garnet produces olivine crystals of Fo_{90} composition. Further dissolution results in the formation of an aggregate of aluminous orthopyroxene and spinel (Fig. 2d). This spinel exhibits a quench texture around the edge of the aggregate.

Textures at 30 kb. At 30 kb, garnet has no reaction texture. All the other four phases exhibit textures characteristic of rapidly quenched glass. Olivine has quench crystals of clinopyroxene with intersertal glass (Fig. 2e). In each case, the width of the zone of quench crystals represents the difference between the original and final crystal/melt interface.

Dissolution rates

The results of the dissolution experiments are given in Table 3 and shown in Figs. 3–5. The results are not conclusive enough to discriminate between time-dependent and time-independent crystal dissolution in these experiments. In order to further investigate this problem, concentration profiles in the glass adjacent to the dissolving crystal were obtained for several experimental durations (Figs. 6–8). The shape and length of the profile and the

TABLE 2

Reaction textures produced during the dissolution experiments

	5 kb	*12 kb*	*30 kb*
Olivine	x	x	q. cpx + gl
Orthopyroxene	ol (Fo_{90}) + chr + gl	x	q. cpx + gl
Clinopyroxene	chr + gl	x	q. cpx + gl
Spinel	v. sp + gl	v. sp + gl	q. + gl
Garnet	—	ol (Fo_{90}) + opx + sp + gl	x

x = no reaction texture, — = no experiment conducted. ol = olivine, chr = chromite, sp = spinel, v. sp = vermicular spinel, gl = glass, opx = orthopyroxene, cpx = clinopyroxene, q = quench texture.

clinopyroxene (augite) is the liquidus phase. In accord with previous studies, the Na_2O and Al_2O_3 content of the clinopyroxene increase with increasing pressure (e.g., Green & Ringwood, 1968; Bultitude & Green, 1971). At 30 kb, the Al_2O_3 content is 14·5 wt. per cent. The liquidus temperatures, bracketed to ± 10 °C, were used to determine the temperatures at which the dissolution experiments were conducted.

Dissolution experiments

Crystal/melt textural relationships

The textures produced during the dissolution experiments are summarized in Table 2.

Textures at 5 kb. In all experiments at 5 kb, olivine crystals have no reaction texture. The dissolution of orthopyroxene produces a thin band of equant chromite crystals at the original crystal/melt interface and further dissolution causes olivine crystals of Fo_{90} composition to crystallize (Fig. 2a). Melt (glass) forms intersertal patches between the olivine crystals. Clinopyroxene also reacts to form a thin layer of chromite crystals at the original interface (Fig. 2b). Thereafter, dissolution of clinopyroxene produces glass only. Spinel dissolution forms a vermicular rim of spinels more Cr- and Fe-rich and less Mg- and Al-rich than the original spinel composition. Irregular patches of glass are trapped between the vermicular crystals (Fig. 2c).

Textures at 12 kb. Olivine, orthopyroxene, and clinopyroxene exhibit no reaction textures. Spinel has a similar vermicular texture to that at 5 kb. Garnet has a complex reaction relationship. Initially, dissolution of garnet produces olivine crystals of Fo_{90} composition. Further dissolution results in the formation of an aggregate of aluminous orthopyroxene and spinel (Fig. 2d). This spinel exhibits a quench texture around the edge of the aggregate.

Textures at 30 kb. At 30 kb, garnet has no reaction texture. All the other four phases exhibit textures characteristic of rapidly quenched glass. Olivine has quench crystals of clinopyroxene with intersertal glass (Fig. 2e). In each case, the width of the zone of quench crystals represents the difference between the original and final crystal/melt interface.

Dissolution rates

The results of the dissolution experiments are given in Table 3 and shown in Figs. 3–5. The results are not conclusive enough to discriminate between time-dependent and time-independent crystal dissolution in these experiments. In order to further investigate this problem, concentration profiles in the glass adjacent to the dissolving crystal were obtained for several experimental durations (Figs. 6–8). The shape and length of the profile and the

TABLE 2

Reaction textures produced during the dissolution experiments

	5 kb	*12 kb*	*30 kb*
Olivine	x	x	q. cpx + gl
Orthopyroxene	ol (Fo_{90}) + chr + gl	x	q. cpx + gl
Clinopyroxene	chr + gl	x	q. cpx + gl
Spinel	v. sp + gl	v. sp + gl	q. + gl
Garnet	—	ol (Fo_{90}) + opx + sp + gl	x

x = no reaction texture, — = no experiment conducted. ol = olivine, chr = chromite, sp = spinel, v. sp = vermicular spinel, gl = glass, opx = orthopyroxene, cpx = clinopyroxene, q = quench texture.

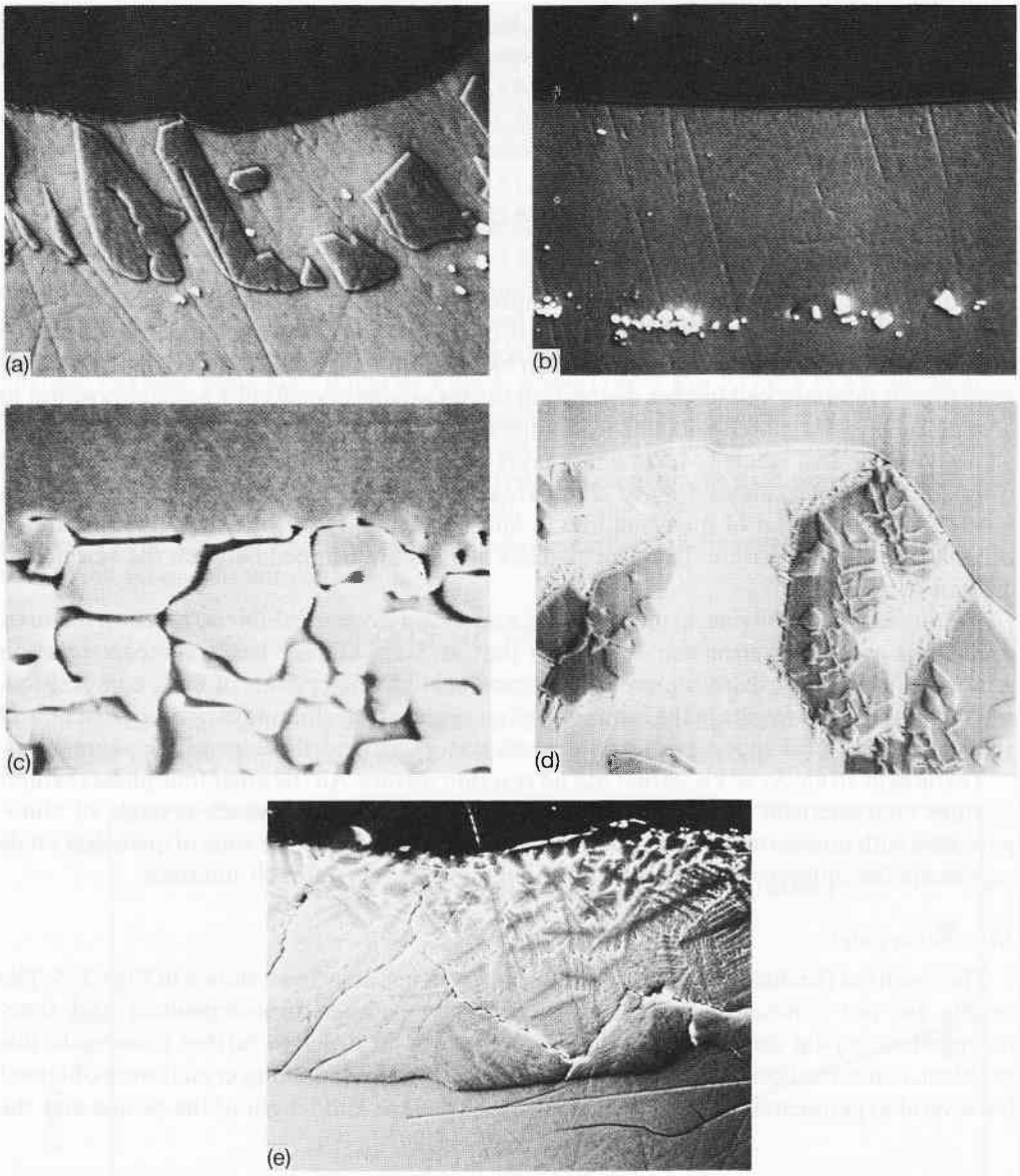

FIG. 2. Back scattered electron images of textures produced during dissolution experiments. Operating conditions: 15 kV accelerating voltage, probe current variable in order to obtain the best image. (a) Orthopyroxene dissolution to olivine + chromite + glass (5 kb, 1300 °C, 30 min). Width of photograph 0·2 mm. (b) Clinopyroxene dissolution to chromite + glass (5 kb, 1300 °C, 30 min). Width of photograph 0·2 mm. (c) Spinel dissolution to spinel + glass (5 kb, 1250 °C, 30 min). Width of photograph 0·02 mm. (d) Garnet dissolution to olivine + orthopyroxene + spinel + glass (12 kb, 1300 °C, 10 min). Width of photograph 0·05 mm. (e) Olivine with quench crystals of clinopyroxene and interstitial glass (30 kb, 1450 °C, 10 min). Width of photograph 0·2 mm.

crystal/melt intercept value for each oxide are identical within analytical error. This suggests that dissolution is time-independent and that steady-state has been achieved (Kuo & Kirkpatrick, 1985). Therefore, the apparent time-dependence in some cases (e.g., clinopyroxene dissolution at 12 kb and 1400 °C; Fig. 4) is probably a function of error in the measurement of the sphere size either before and/or after the experiment. Finally, in order to determine the

Run no.
02SP
03OL
04SP
04GT
04EN
05DI
07OL
07SP
07GT
08OL
08GT
08SP
09OL(1)
09OL(2)
10EN
10DI
11EN
12OL
12GT
12SP
13OL
14GT
14SP
19GT
21DI
22OL
23OL
25DI
27SP
28EN
30DI
31OL
32EN
32DI
35OL
35SP
35GT
37OL
38SP
40SP
43OL
44SP
47SP
48GT
49GT
50GT
52EN
52DI
53EN
53DI
54EN
54DI
55OL
55SP
56EN
56DI
57OL
57SP
59OL

nts. Operating conditions:
Orthopyroxene dissolution
inopyroxene dissolution to
tion to spinel + glass (5 kb,
opyroxene + spinel + glass
tals of clinopyroxene and
2 mm.

l error. This suggests
hieved (Kuo & Kirk-
s (e.g., clinopyroxene
r in the measurement
rder to determine the

TABLE 3

Results of dissolution experiments

Run no.	P (*kb*)	T (°*C*)	r_i (*cm*)	r_f (*cm*)	Δr (*cm*)	t (*s*)
02SP	30	1500	0·033	0·022 ± 0·002	0·011 ± 0·002	1800
03OL	30	1500	0·058	0·039	0·019	600
04SP	30	1500	0·037	0·035	0·002	600
04GT			0·048	0·025	0·023	
04EN			0·045 ± 0·002	0·037	0·008 ± 0·002	
05DI	30	1500	0·041 ± 0·002	0·026 ± 0·002	0·015 ± 0·002	600
07OL	30	1450	0·054 ± 0·002	0·054 ± 0·002	0·000 ± 0·002	600
07SP			0·037	0·037	0·000	
07GT			0·040	0·035	0·005	
08OL	30	1450	0·068	0·058 ± 0·002	0·010 ± 0·002	1800
08GT			0·042	0·029 ± 0·003	0·013 ± 0·003	1800
08SP			0·037	0·036	0·001	
09OL(1)	30	1450	0·069 ± 0·002	0·058 ± 0·002	0·011 ± 0·002	1800
09OL(2)			0·058	0·048	0·010	
10EN	30	1450	0·036	0·031 ± 0·002	0·005 ± 0·002	600
10DI			0·036 ± 0·002	0·033 ± 0·002	0·003 ± 0·002	
11EN	30	1450	0·050	0·043	0·007	1800
12OL	30	1450	0·073	0·054 ± 0·002	0·019 ± 0·002	3600
12GT			0·049 ± 0·002	0·027 ± 0·002	0·022 ± 0·002	
12SP			0·037	0·034 ± 0·002	0·003 ± 0·002	
13OL	30	1450	0·084 ± 0·002	0·046 ± 0·002	0·038 ± 0·002	7200
14GT	30	1450	0·053 ± 0·002	0·018	0·035 ± 0·002	7200
14SP			0·052	0·048	0·004	
19GT	30	1500	0·072 ± 0·002	D	> 0·072 ± 0·002	1800
21DI	30	1450	0·039 ± 0·002	0·038	0·001 ± 0·002	1800
22OL	30	1450	0·053	0·043 ± 0·002	0·010 ± 0·002	1500
23OL	30	1450	0·048 ± 0·002	0·038 ± 0·002	0·010 ± 0·002	1500
25DI	30	1450	0·034 ± 0·002	0·029	0·005 ± 0·002	3600
27SP	30	1500	0·054	0·014	0·040	7200
28EN	30	1450	0·050	0·034 ± 0·002	0·016 ± 0·002	3600
30DI	30	1450	0·036 ± 0·002	0·030 ± 0·002	0·006 ± 0·002	7200
31OL	30	1500	0·086	0·081 ± 0·002	0·005 ± 0·002	300
32EN	30	1500	0·050 ± 0·002	0·030	0·020 ± 0·002	1800
32DI			0·034 ± 0·002	D	> 0·034 ± 0·002	
35OL	12	1300	0·045	0·043	0·002	1800
35SP			0·031	0·030	0·001	
35GT			0·042	D	> 0·042	
37OL	12	1300	0·047	0·044	0·003	3600
38SP	12	1300	0·037	0·037	0·000	3600
40SP	12	1300	0·039	0·038	0·001	7200
43OL	12	1350	0·049	0·048	0·001	1200
44SP	12	1350	0·030	0·030	0·000	1800
47SP	12	1400	0·038	0·037	0·001	1800
48GT	12	1300	0·054 ± 0·002	D	> 0·054 ± 0·002	1200
49GT	12	1300	0·057	0·047	0·010	600
50GT	12	1400	0·079 ± 0·002	D	> 0·079 ± 0·002	600
52EN	12	1300	0·043	0·041	0·002	1800
52DI			0·039 ± 0·002	0·039 ± 0·002	0·000 ± 0·002	
53EN	12	1400	0·065	0·060	0·005	1800
53DI			0·043	0·028	0·015	
54EN	12	1350	0·044	0·039	0·005	1800
54DI			0·029	0·026	0·003	
55OL	12	1400	0·059 ± 0·002	0·049	0·010 ± 0·002	3600
55SP			0·041	0·041	0·000	
56EN	12	1300	0·035	0·031	0·004	7200
56DI			0·030	0·029	0·001	
57OL	12	1350	0·048	0·044	0·004	3600
57SP			0·029	0·029	0·000	
59OL	12	1400	0·052	0·043	0·009	1800

TABLE 3 (*cont.*)

Run no.	P (*kb*)	T (°C)	r_i (*cm*)	r_f (*cm*)	Δr (*cm*)	t (*s*)
60SP	12	1400	0·038	0·036	0·002	3600
61EN	12	1300	0·034	0·032	0·002	3600
61DI			0·029	0·028	0·001	3600
62EN	12	1350	0·048 ± 0·002	0·041	0·007 ± 0·002	3600
62DI			0·031	0·026	0·005	
63EN	12	1400	0·061	0·051	0·010	3600
63DI			0·043	0·024	0·019	
64OL	12	1300	0·045	0·041	0·004	7200
64SP			0·026	0·026	0·000	
65OL	12	1350	0·052	0·044	0·008	7200
65SP			0·031	0·030	0·001	
66OL	12	1400	0·054 ± 0·002	0·032	0·022 ± 0·002	7200
66SP			0·042 ± 0·002	0·040	0·002 ± 0·002	
67OL	12	1400	0·051 ± 0·002	0·039	0·012 ± 0·002	3600
68OL(1)	12	1400	0·044	0·036	0·008	3600
68OL(2)			0·031	0·019	0·012	
69OL(1)	12	1400	0·041 ± 0·002	0·027	0·014 ± 0·002	3600
69OL(2)			0·036	0·022	0·014	
70OL(1)	12	1400	0·061	0·050 ± 0·002	0·011 ± 0·002	3600
70OL(2)			0·024	0·008	0·016	3600
71OL(1)	12	1400	0·042	0·035	0·007	3600
71OL(2)			0·028	0·012	0·016	
72OL(1)	12	1400	0·037	0·024	0·013	3600
72OL(2)			0·032	0·017	0·015	
73OL	5	1250	0·033	0·032	0·001	1800
73SP			0·030	0·030	0·000	
74EN	5	1250	0·037 ± 0·002	0·035	0·002 ± 0·002	1800
74DI			0·040 ± 0·002	0·036	0·004 ± 0·002	
75OL	5	1300	0·030	0·029	0·001	1800
75SP			0·029	0·029	0·000	
76EN	5	1300	0·034	0·030	0·004	1800
76DI			0·031	0·024	0·007	
77OL	5	1250	0·031	0·030	0·001	3600
77SP			0·023	0·023	0·000	
78EN	5	1250	0·035	0·029	0·006	3600
78DI			0·028	0·024	0·004	3600
79OL	5	1300	0·029	0·027	0·002	3600
79SP			0·025	0·023	0·002	
80EN	5	1300	0·034	0·027	0·007	3600
80DI			0·028	0·008	0·020	
81OL	5	1250	0·022	0·021	0·001	7200
81SP			0·022	0·021	0·001	
82EN	5	1250	0·036	0·029	0·007	7200
82DI			0·032	0·020	0·012	
83OL	5	1300	0·026	0·019	0·007	7500
83SP			0·026	0·023	0·003	
84EN	5	1300	0·046	0·029	0·017	7200
84DI			0·043	0·009	0·034	
85OL	12	1400	0·026	0·023	0·003	600
85DI			0·027	0·021	0·006	
86OL	12	1400	0·041	0·035	0·006	1200
86DI			0·032	0·020	0·012	

OL = olivine, SP = spinel, DI = chrome diopside, EN = orthopyroxene, GT = garnet. r_i = initial radius of sphere, r_f = final radius of sphere, Δr = change in sphere radius. D = sphere completely dissolved. Errors are ±0·001 cm unless otherwise stated.

FIG. 3. Change in
Error bars on the
experiment. The

effect of the
melt region.
The dissolu
data points
dissolution
the rate of di
was estimated
gas systems

The use and

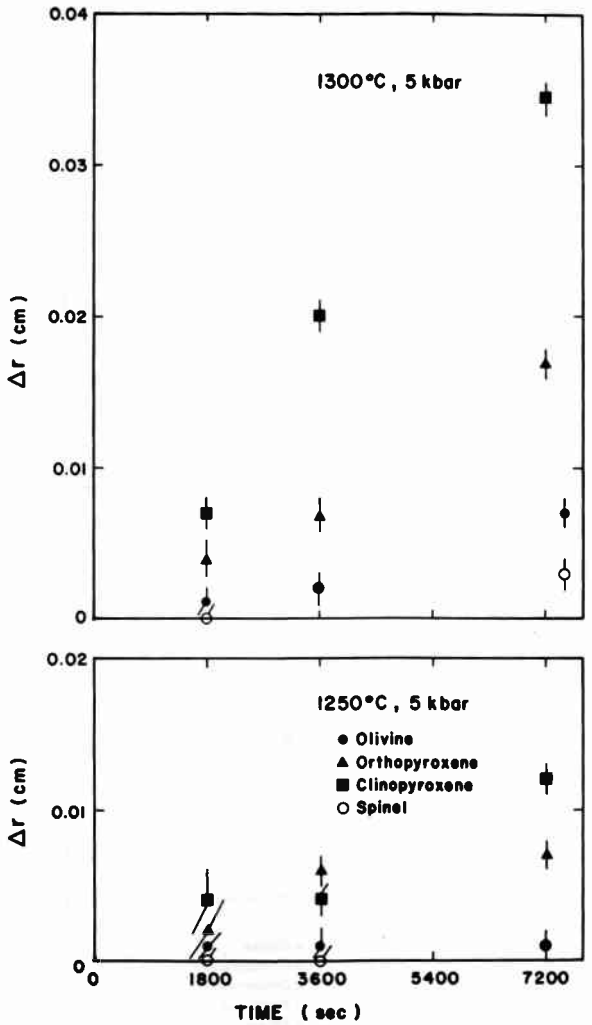

FIG. 3. Change in radius (in cm) of crystals against time for experiments at 5 kb and the temperatures indicated. Error bars on the individual points represent estimated errors during measurement of spheres before and after the experiment. The dissolution rate is calculated by a linear least-squares regression fit through the data points with a weighted value assigned to the origin (Table 4).

effect of the run-up on the dissolution rate, several experiments were performed in the partial melt region. No dissolution was observed.

The dissolution rates were calculated by a linear least-squares regression fit through the data points with a weighted value assigned to the origin, because there is clearly no dissolution possible at zero time. The results are shown in Table 4 and Fig. 9. In cases where the rate of dissolution is slow and cannot be resolved from Figs. 3 and 4, the dissolution rate was estimated according to the following equation derived for bubble dissolution in liquid–gas systems (Epstein & Plesset, 1950):

$$\left(\frac{r}{r_i}\right)^2 = 1-\left[\frac{2Dt(c_s-c_i)}{\rho r_i^2}\right]. \quad (1)$$

The use and applicability of this equation has been discussed by Harrison & Watson (1984),

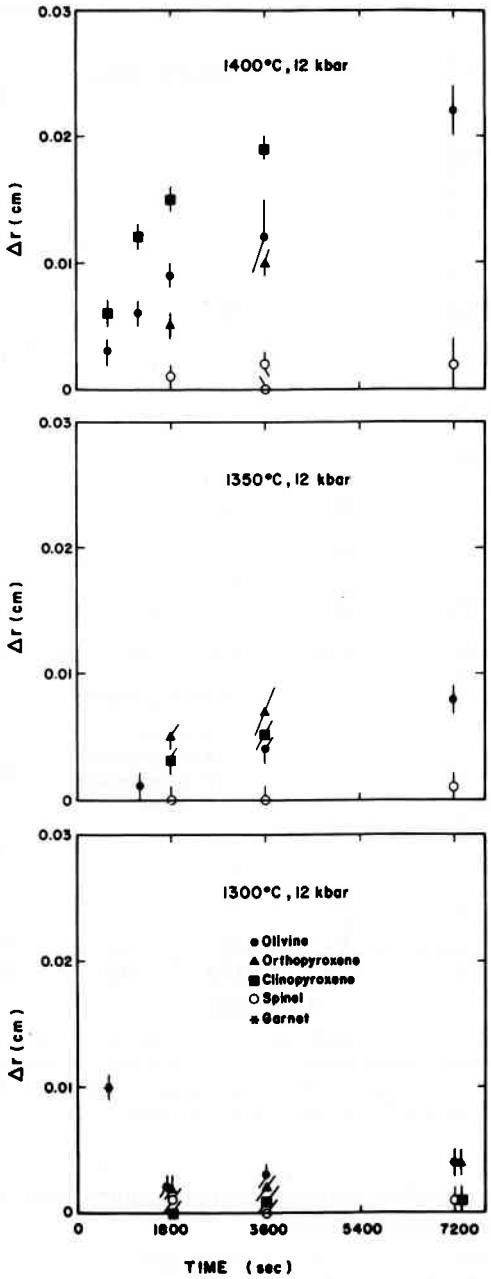

FIG. 4. Change in radius (in cm) of crystals against time for experiments at 12 kb and the temperatures indicated. See Fig. 3 for details of error bars and the calculation of dissolution rates.

who used it to calculate the dissolution rate of apatite in granitic melts. They noted that the equation gave very similar results to, and is easier to use than, the more commonly employed equation developed for heat transfer (Carslaw & Jaeger, 1959). In equation (1), r_i is the initial radius of the sphere, r is the final radius, t is time, c_s is the equilibrium saturation composition at the crystal/melt interface, c_i is the initial concentration of the relevant species and ρ is the

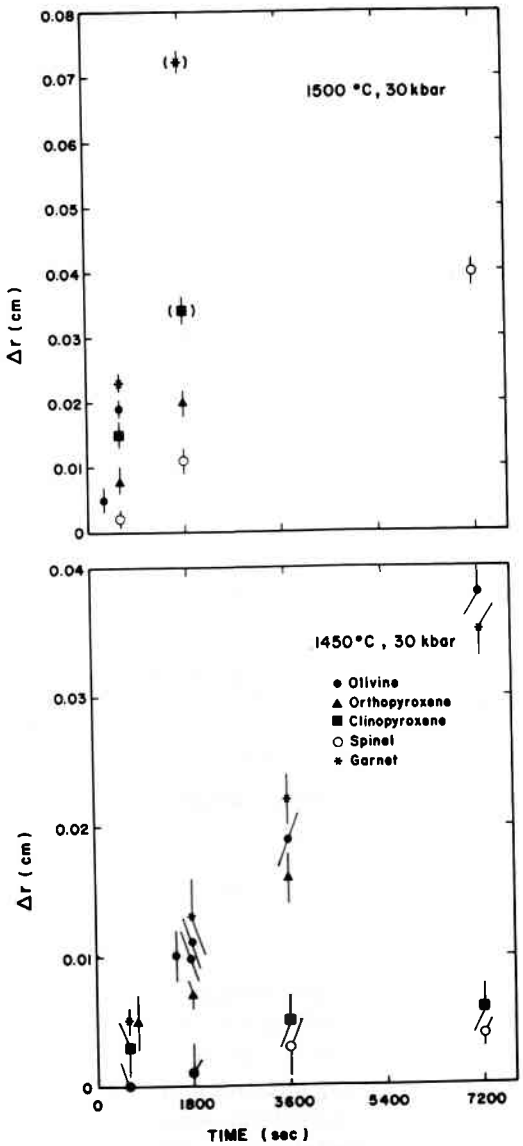

FIG. 5. Change in radius (in cm) of crystals against time for experiments at 30 kb and the temperatures indicated. Points with parentheses represent experiments where the sphere completely dissolved.

density of the bubble forming species. This latter parameter may be replaced by the density of the crystal multiplied by the approximate volume fraction of the relevant species in the crystal (Harrison & Watson, 1984). D is the diffusion coefficient of the relevant species calculated from the following solution to the diffusion equation:

$$\frac{c_x - c_i}{c_s - c_i} = \text{erfc}\left(\frac{x}{2\sqrt{Dt}}\right) \tag{2}$$

(Crank, 1975). Here, c_x is the concentration at distance x from the interface and erfc is the error function complement. In order to estimate the dissolution rate, the diffusivity of the

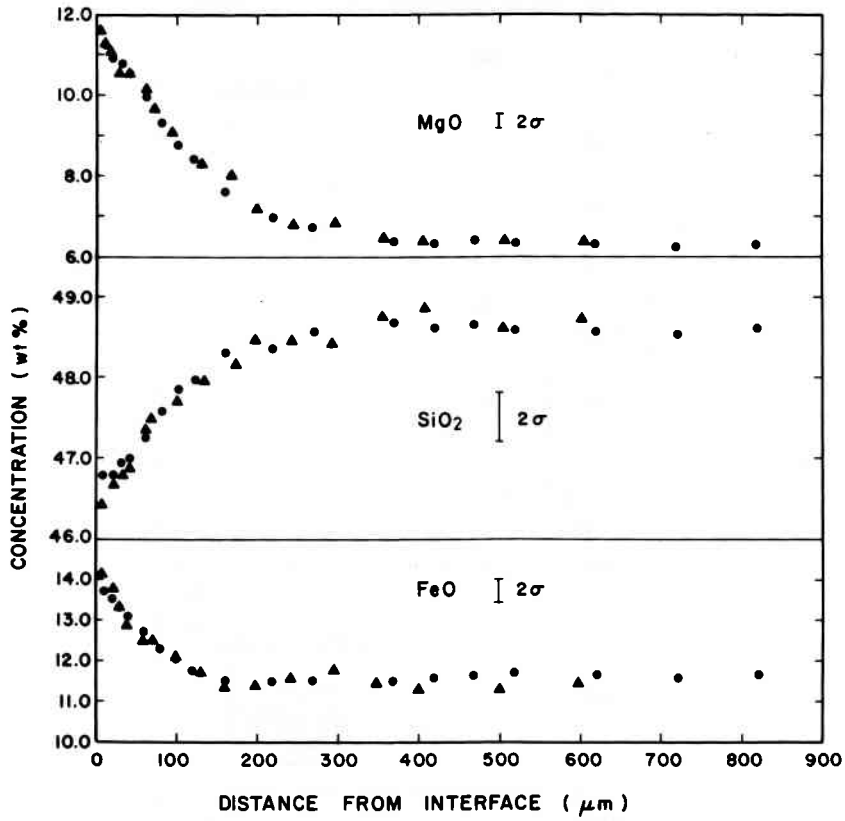

FIG. 6. Concentration profiles of the major elements in the glass adjacent to dissolving olivine crystals. Experiments made at 12 kb and 1400 °C. Filled circles represent experiment of 60 min duration. Triangles represent experiment of 10 min duration.

least mobile species in the melt was utilized in each case. It should be noted that the error function approximation is a less than satisfactory fit to the concentration profile because of the presence of a moving interface. However, in cases where the dissolution rate is demonstrably slow, the effect of a moving interface may be neglected because the movement of the crystal/melt boundary is small relative to the length of the profile (Harrison & Watson, 1984). The effect of a moving interface in calculating diffusion coefficients is considered later. The parameters used in the estimation of dissolution rates using equation (1) are given in Table 4. If the experimental duration $t \ll \rho r_i^2/2D(c_s - c_i)$, then equation (1) indicates there will be little change of the dissolution rate with time and steady-state is approximated. The results of the calculations are also plotted in Fig. 9.

Dissolution at 5 kb. At 5 kb, the rates of dissolution of olivine, orthopyroxene, clinopyroxene, and spinel were determined at 1250 and 1300 °C (equivalent to superheatings of 25 and 75 °C, respectively). The dissolution rates at both temperatures decrease in the order clinopyroxene > orthopyroxene > olivine > spinel. The temperature dependence of dissolution of each mineral may be fitted to an Arrhenius equation of the form:

$$u = u_o \exp\left(\frac{E_u}{RT}\right) \tag{3}$$

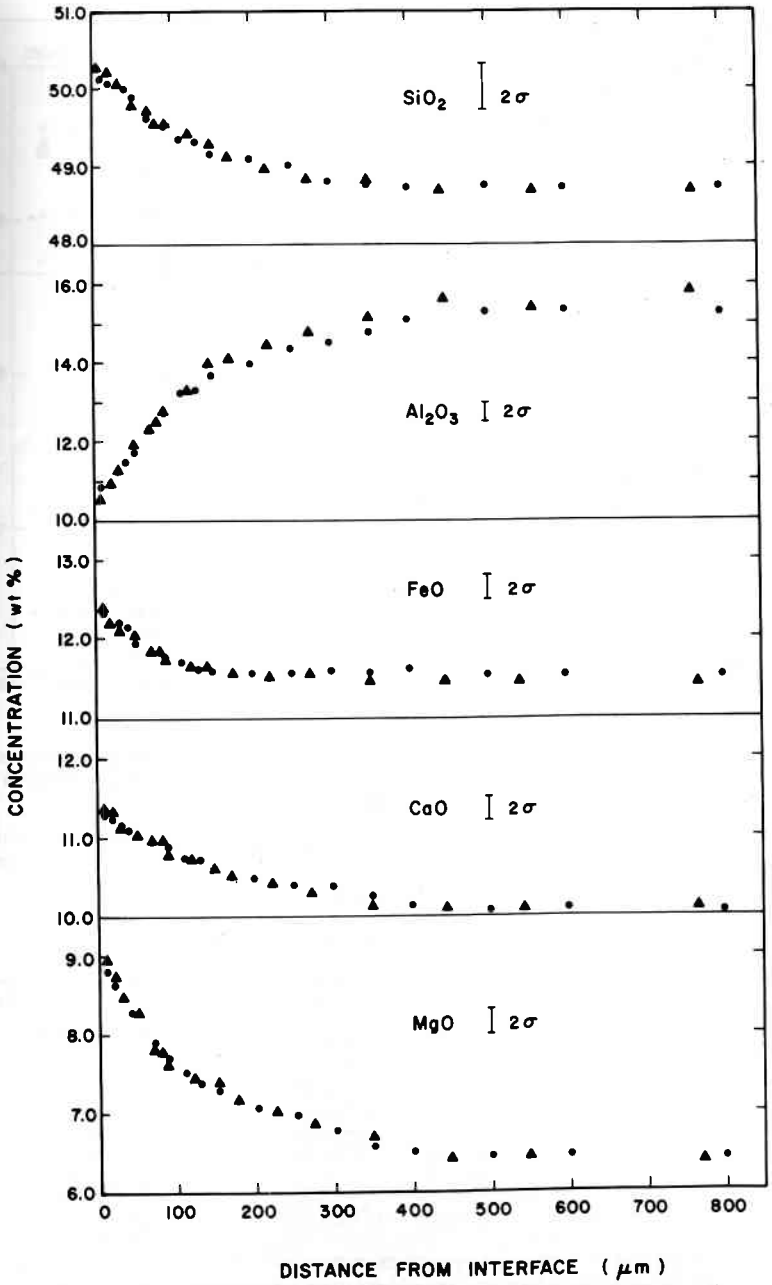

FIG. 7. Concentration profiles of the major elements in the glass adjacent to dissolving clinopyroxene crystals. Experiments made at 5 kb and 1250 °C. Filled circles represent experiment of 30 min duration. Triangles represent experiment of 60 min duration.

where u is the dissolution rate, u_o is a constant, E_u is the activation energy of dissolution, R is the gas constant and T is absolute temperature. Because only two temperatures were investigated at 5 kb, the calculated activation energies are subject to large errors. However, it is probable that olivine and spinel have significantly larger activation energies than either orthopyroxene or clinopyroxene (Table 5).

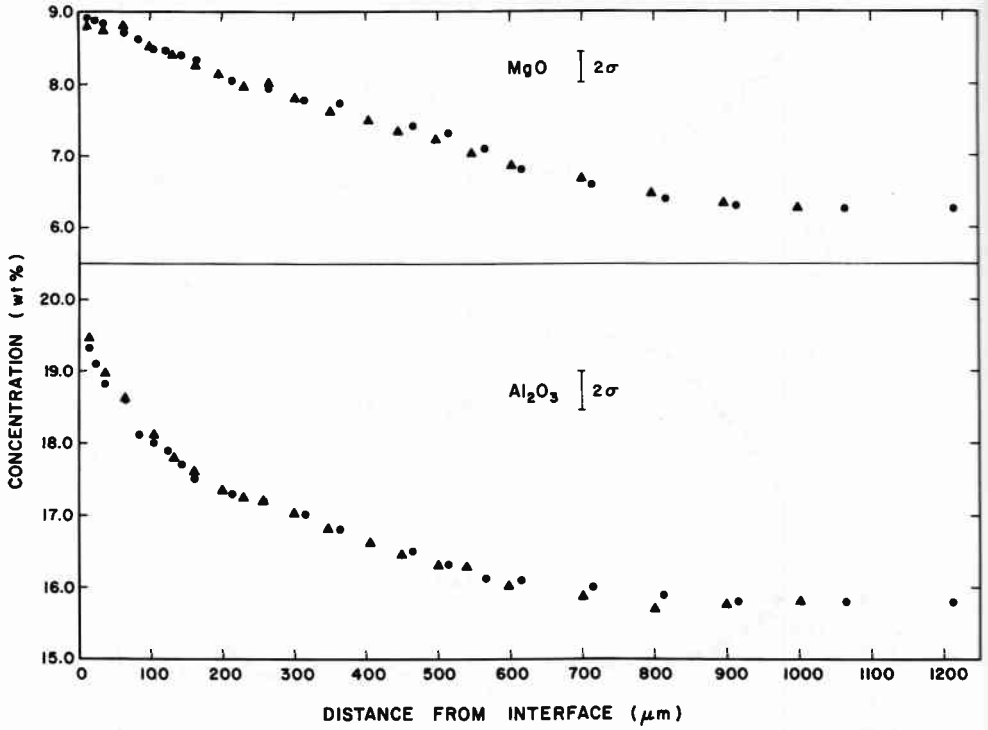

FIG. 8. Concentration profiles of the major elements in the glass adjacent to dissolving spinel crystals. Experiments made at 30 kb and 1450 °C. Filled circles represent experiment of 30 min duration. Triangles represent experiment of 120 min duration.

TABLE 4

Mineral dissolution rates (cm s^{-1})

	5 kb		*12 kb*			*30 kb*	
	1250 °C	*1300 °C*	*1300 °C*	*1350 °C*	*1400 °C*	*1450 °C*	*1500 °C*
Olivine	$2{\cdot}09 \times 10^{-8}$	$8{\cdot}51 \times 10^{-7}$	$6{\cdot}33 \times 10^{-7}$	$1{\cdot}11 \times 10^{-6}$	$3{\cdot}24 \times 10^{-6}$	$5{\cdot}35 \times 10^{-6}$	$3{\cdot}17 \times 10^{-5}$
Orthopyroxene	$1{\cdot}51 \times 10^{-6}$	$2{\cdot}28 \times 10^{-6}$	$5{\cdot}81 \times 10^{-7}$	$2{\cdot}11 \times 10^{-6}$	$2{\cdot}78 \times 10^{-6}$	$4{\cdot}35 \times 10^{-6}$	$1{\cdot}13 \times 10^{-5}$
Clinopyroxene	$1{\cdot}11 \times 10^{-6}$	$4{\cdot}84 \times 10^{-6}$	$1{\cdot}59 \times 10^{-7}$	$1{\cdot}44 \times 10^{-6}$	$6{\cdot}27 \times 10^{-6}$	$9{\cdot}05 \times 10^{-7}$	$2{\cdot}50 \times 10^{-5}$
Spinel	$9{\cdot}21 \times 10^{-9}$	$4{\cdot}10 \times 10^{-7}$	$4{\cdot}21 \times 10^{-8}$	$1{\cdot}11 \times 10^{-7}$	$2{\cdot}88 \times 10^{-7}$	$6{\cdot}05 \times 10^{-7}$	$5{\cdot}58 \times 10^{-6}$
Garnet	—	—	1.67×10^{-5}	—	—	$5{\cdot}13 \times 10^{-6}$	$3{\cdot}83 \times 10^{-5}$

Underlined dissolution rates are calculated using equation (1). Parameters used are as follows: olivine, $\rho = 1{\cdot}32$ g cm^{-3}, $D(SiO_2) = 1{\cdot}58 \times 10^{-8}$ cm^2 s^{-1}, $(c_s - c_i) = 0{\cdot}0435$ g cm^{-3}, spinel (1250 °C, 5 kb), $\rho = 2{\cdot}4$ g cm^{-3}, $D(Al_2O_3) = 1{\cdot}5 \times 10^{-8}$ cm^2 s^{-1}, $(c_s - s_i) = 0{\cdot}048$ g cm^{-3}, spinel (1300 °C, 12 kb), $\rho = 2{\cdot}4$ g cm^{-3}, $D(Al_2O_3) = 4{\cdot}95 \times 10^{-8}$ cm^{-2} s^{-1}, $(c_s - c_i) = 0{\cdot}051$ g cm^{-3}, spinel (1350 °C, 12 kb), $\rho = 2{\cdot}4$ g cm^3, $D(Al_2O_3) = 8{\cdot}2 \times 10^{-8}$ cm^2 s^{-1}, $(c_s - c_i) = 0{\cdot}081$ g cm^{-3}.

See text for discussion of estimation of $= \rho$. Melt densities for c_s and c_i estimated from Herzberg (1986).

Dissolution at 12 kb. At 12 kb, the dissolution rates of olivine, orthopyroxene, clinopyroxene, and spinel were determined at 1300, 1350 and 1400 °C (25, 75 and 125 °C superheating, respectively). The dissolution rate of garnet is very rapid at this pressure such that only one experiment of 10 min duration was successful at 1300 °C. All other experiments resulted in the complete dissolution of garnet (Table 3). The dissolution rate of spinel is slowest at each temperature. At 1300 °C, the order of dissolution is olivine+

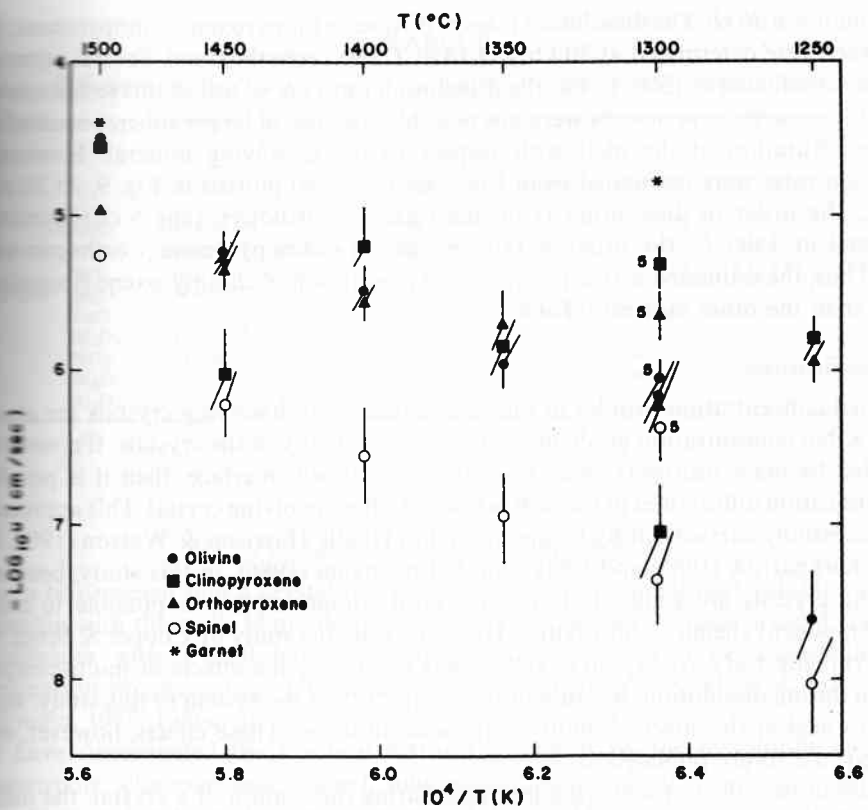

Logarithm of the dissolution rate taken from Figs. 3–5 v. reciprocal temperature. Error bars represent estimated errors in the best fit lines from Figs. 3–5 propagated through the calculations. Numbers on the data points at 1300 °C represent the dissolution rate at 5 kb.

TABLE 5

Activation energies (kcal mol^{-1}) of dissolution at each pressure

	5 kb	*12 kb*	*30 kb*
Olivine	335 ± 16/28	84 ± 6	210 ± 14/42
Orthopyroxene	66 ± 5	85 ± 6/24	112 ± 42
Clinopyroxene	111 ± 12	223 ± 40/35	420 ± 55/43
Spinel	357 ± 16/55	96 ± 5	280 ± 41/56
Garnet			252 ± 28/56

Calculations at 5 and 30 kb based on two temperatures. ±28/56 refers to the error (+28, −56 kcal mol^{-1}) calculated by fitting a line through the error bars on the individual dissolution rates.

orthopyroxene > clinopyroxene > spinel; whereas at 1400 °C, the order of dissolution is clinopyroxene > olivine + orthopyroxene > spinel (Fig. 9). These dissolution rates were fitted to the Arrhenius equation (3) by least-squares regression. Activation energies for dissolution were calculated as 84 ± 6, 85 ± 6, 223 ± 40 and 96 ± 5 kcal mol^{-1} for olivine, orthopyroxene, clinopyroxene, and spinel, respectively.

Type A dissolu
30 kb). Type B
The presence o
reference to the
subliquidus phas
thus precluding a
phase equilibria
sequence may b
pressure clinopy
At 5 kb, olivin
t is more Mg-rich
phases are less
clinopyroxene,
released from the
he melt. The lack

ype A dissolutio
0 kb). Type B d
The presence o
eference to the
ubliquidus phas
hus precluding a
hase equilibria
equence may b
ressure clinopy
At 5 kb, olivine
t is more Mg-ric
hases are less
linopyroxene, c
eleased from the
he melt. The lack

Dissolution at 30 kb. The dissolution rates of olivine, orthopyroxene, clinopyroxene, spinel, and garnet were determined at 30 kb and 1450 °C (60 ° superheating). Several experiments were also conducted at 1500 °C, but the dissolution rates are so fast at this temperature that detailed time-series experiments were not possible, and use of larger spheres resulted in the possible saturation of the melt with respect to the dissolving mineral. However, the dissolution rates were calculated from Fig. 5 and are also plotted in Fig. 9, At 30 kb and 1450 °C, the order of dissolution is olivine + garnet + orthopyroxene > clinopyroxene > spinel and at 1500 °C, the order is olivine + garnet + clinopyroxene > orthopyroxene > spinel. Thus, the estimated activation energy of dissolution of clinopyroxene is significantly greater than the other minerals (Table 5).

Cation diffusivities

Selected concentration profiles in the glass adjacent to dissolving crystals are shown in Figs. 6–8. No concentration gradients were observed in any of the crystals. If dissolution is controlled by mass transport away from the crystal/melt interface, then it is possible to determine cation diffusivities in the melt adjacent to the dissolving crystal. This approach has been successfully carried out by Cooper & Schut (1980), Harrison & Watson (1983, 1984), Kuo & Kirkpatrick (1985) and Chekhmir & Epel'baum (1986). In this study, because the dissolving crystals are solid solutions of several components, it is possible to measure multi-component chemical diffusivities. However, only the study by Cooper & Schut (1980) in the synthetic CaO–Al_2O_3–SiO_2 system has dealt with the effects of multi-component diffusion during dissolution. Because of the complexity of the system in this study, we have chosen to neglect the effect of multi-component diffusion. These effects, however, will be evaluated in a future publication.

Because of the effect of a moving interface during dissolution of a crystal, the diffusion equation for the steady-state case is:

$$D \cdot \frac{d^2c}{dx^2} + u \cdot \frac{dc}{dx} = 0 \qquad (4)$$

subject to the boundary conditions $c_L = c_i$ at $x = \infty$ and $c_L = c_i/k$ at $x = 0$ (Kuo & Kirkpatrick, 1985). The solution to this equation has been derived by Smith *et al.* (1955):

$$\frac{c_L}{c_i} = 1 + \left(\frac{1-k}{k}\right) \exp\left[\frac{(-ux)}{D}\right] \qquad (5)$$

where c_L is the concentration of a particular species in the melt at distance x from the crystal/melt interface, c_i is the initial concentration of the species in the melt, $k\,(= c_i/c_L)$ is the crystal/melt distribution coefficient, u is the dissolution rate, and D is the diffusion coefficient.

The results of the calculation of single-component diffusivities for olivine, spinel, and clinopyroxene dissolution are shown in Table 6. The most important point to note here is that the apparent diffusivities appear to show a positive correlation with the dissolution rate of the mineral, which should not be the case if diffusion is the only rate-controlling process. For example, at 1400 °C and 12 kb, the diffusion coefficient calculated for MgO is $2{\cdot}85 \times 10^{-$ for spinel dissolution, $5{\cdot}18 \times 10^{-8}$ for olivine dissolution and $1{\cdot}02 \times 10^{-7}$ for clinopyroxene dissolution. The dissolution rates of the three minerals decrease in the order clinopyroxene > olivine > spinel at this temperature and pressure. Therefore, it is possible that dissolution is controlled by a mixed process involving both diffusion and interface reaction. It may also be an indication that multi-component effects and the speciation of diffusing components in the melt play an important role. Similar conclusions can be drawn for cation diffusivities at any temperature and pressure (cf. Tables 4 and 6).

TABLE 6

Diffusion coefficients ($cm^2\ s^{-1}$) calculated for single-component oxides

		5 kb		12 kb			30 kb	
		1250 °C	1300 °C	1300 °C	1350 °C	1400 °C	1450 °C	1500 °C
Olivine	MgO	1.91×10^{-9}	1.21×10^{-8}	7.79×10^{-9}	1.38×10^{-8}	5.18×10^{-8}	1.78×10^{-7}	1.45×10^{-6}
	FeO	1.25×10^{-9}	6.25×10^{-9}	3.95×10^{-9}	1.18×10^{-8}	2.34×10^{-8}	4.62×10^{-8}	2.75×10^{-7}
	SiO_2	1.79×10^{-9}	8.01×10^{-9}	3.79×10^{-9}	6.88×10^{-9}	3.13×10^{-8}	4.47×10^{-8}	1.78×10^{-7}
Clinopyroxene	MgO	1.51×10^{-8}			1.98×10^{-8}	1.02×10^{-7}		
	CaO	2.78×10^{-8}			2.72×10^{-8}	1.32×10^{-7}		
	Al_2O_3	1.25×10^{-8}			1.54×10^{-8}	6.98×10^{-8}		
	SiO_2	1.01×10^{-8}			1.64×10^{-8}	3.02×10^{-8}		
Spinel	MgO		3.82×10^{-9}	9.50×10^{-10}	1.63×10^{-9}	2.83×10^{-9}	3.02×10^{-8}	1.56×10^{-7}
	Al_2O_3		4.60×10^{-9}	3.50×10^{-10}	1.69×10^{-9}	3.62×10^{-9}	1.07×10^{-8}	8.50×10^{-8}

DISCUSSION

Crystal/melt textural relationships

It is to be expected that a crystal not in equilibrium with a melt may exhibit a reaction relationship with the melt. Many natural examples of reaction coronas around crystals in disequilibrium with a melt have been attributed to magma mixing, assimilation or contamination processes (e.g., Hibbard, 1981; Sakuyama, 1981; Gerlach & Grove, 1982; Tsuchiyama, 1985, 1986*a*, *b*).

We have documented the reaction textures produced by the dissolution of olivine, orthopyroxene, clinopyroxene, spinel, and garnet in an alkali basalt at *superliquidus* temperatures and at three different pressures (Table 2). The crystal/melt textural relationships observed in this study may be grouped into two categories:

(1) Type A dissolution (simple dissolution of Tsuchiyama, 1985) characterized by the reaction:

$$\text{crystal} + \text{melt}_1 \rightarrow \text{melt}_2;$$

(2) Type B dissolution (partial dissolution of Tsuchiyama, 1985) characterized by the reaction:

$$\text{crystal}_1 + \text{melt}_1 \rightarrow \text{crystal}_2 + \text{melt}_2.$$

Type A dissolution occurs at all three pressures studied (e.g., olivine at 5 and 12 kb, garnet at 30 kb). Type B dissolution occurs at 5 kb (e.g., orthopyroxene) and 12 kb (e.g., garnet).

The presence of crystal/melt textures at superliquidus temperatures may be discussed with reference to the liquidus phase diagram of the alkali basalt (Fig. 1). Unfortunately, subliquidus phase relationships have not been determined for this alkali basalt composition, thus precluding a detailed examination of relative mineral stabilities with textures. However, phase equilibria of similar compositions indicate that at low pressure the crystallization sequence may be olivine → clinopyroxene + plagioclase ± orthopyroxene and at higher pressure clinopyroxene → garnet ± orthopyroxene (Basaltic Volcanism Study Project, 1981).

At 5 kb, olivine shows no reaction texture both because it is the liquidus phase and because it is more Mg-rich than the equilibrium olivine composition (Tsuchiyama, 1986*a*). All other phases are less stable and therefore exhibit reaction textures. The initial reaction of clinopyroxene, orthopyroxene and spinel to produce chromite suggests that the Cr_2O_3 released from these mineral phases during dissolution causes local saturation of chromite in the melt. The lack of chromite crystallization after this stage may be due to the change in melt

The binary system diop
(u_{An}) vs. diopside (u_{Di}) i
melt composition

elated study, Kuo d
enstatite and dio
vely explained by
cally in Fig. 11. Th
ectic melt composi
asily be used qua
rated qualitatively
dissolution rate

related study, Kuo
enstatite and di
ively explained by
ically in Fig. 11. T
eutectic melt compo
easily be used qu
demonstrated qualitativel
relative dissolution ra

raphite. Further dissolution of clinopyroxene is of Type A, suggesting that clinopyroxene i elatively stable. The crystallization of olivine by dissolution of orthopyroxene also indicate hat olivine is the most stable phase at this pressure.

The absence of reaction textures during the dissolution of olivine, orthopyroxene, an linopyroxene at 12 kb suggests that these three phases are stable at or just below th quidus. Garnet is clearly not stable at this pressure and crystallizes a variety of minerals as issolves. The initial rapid release of Mg from the garnet probably causes olivine saturatio Thereafter, the transport of other cations away from the interface results in the crystallizatio f orthopyroxene and spinel. Hunter & Taylor (1982) have observed the reactio yrope → spinel + clinopyroxene + orthopyroxene in a symplectite intergrowth with glas ± olivine in a natural kimberlite. This reaction is very similar to the dissolution reactio locumented here.

At 30 kb, quench textures are present around all the dissolving phases except garnet, whic lissolves by simple dissolution at this pressure. Quench textures have been documented i nany experimental studies at high pressure (e.g., Elthon & Scarfe, 1984; Takahashi & Scarf 985). However, the textures formed in this study only occur in the volume of melt betwee he original and final crystal/melt interface, indicating the more Mg-rich composition of th one.

Dissolution rates

The dissolution rates of olivine, orthopyroxene, clinopyroxene, spinel and garn letermined in this study are shown in Fig. 10 together with other data relevant to

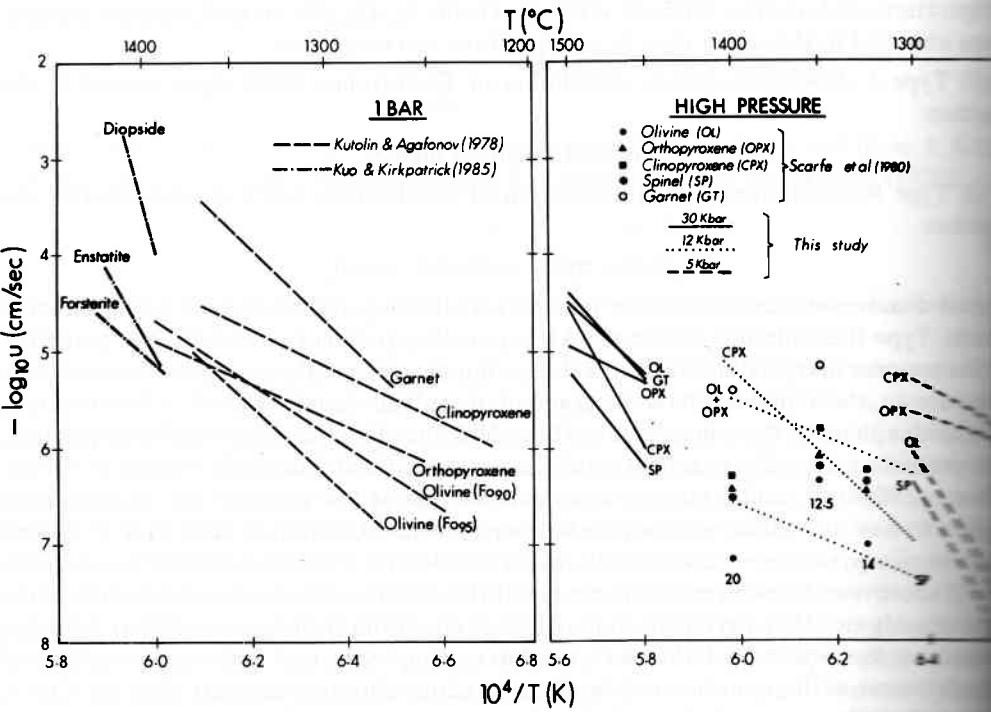

FIG. 10. Logarithm of the dissolution rate vs. reciprocal temperature at 1 b and high pressure. Lines pressure diagram from this study are taken from Fig. 9

dissolution of mane
Scarfe *et al.*, 1980; Ku
Thornber & Huebner

Dissolution at 1 b

The dissolution rates
1 b by Kutolin & Agaf
degrees of superheatin
olivine of Fo_{95} composi
It may therefore be con
at the slowest rate and
than Fo_{90}) may dissolv
statement was confirm
dissolve faster than oli
equilibrium olivine co
considering the simple
liquidus, more Mg-rich
likely to dissolve at a s

Kutolin & Agafonov
a much faster rate tha
activation energy for d
appears that the dissolu
Fig. 10).

(°C)

of mafic minerals in mafic melts at various pressures (Kutolin & Agafonov, 1978; *et al.* 1980; Kuo & Kirkpatrick, 1985). The data of Donaldson (1984, 1985) and & Huebner (1985) have been omitted from Fig. 10 for clarity.

at 1 b

The dissolution rates of upper mantle minerals in an alkalic melt have been determined at Kutolin & Agafonov (1978). Their results show that the order of dissolution at small of superheating is garnet > clinopyroxene > orthopyroxene > olivine, and that of Fo_{95} composition dissolves at a slower rate than does olivine of Fo_{90} composition. therefore be concluded that the mineral phase which is stable on the liquidus dissolves the slowest rate and that the equilibrium olivine composition (presumably less Mg-rich than Fo_{90}) may dissolve at a faster rate than more Mg-rich olivine compositions. This latter ment was confirmed by Donaldson (1984), who concluded that phenocryst olivines solve faster than olivines which are more magnesian. The preferential dissolution of uilibrium olivine compositions relative to Mg-rich olivines may be explained by sidering the simple forsterite–fayalite binary loop. At isothermal conditions above the uidus, more Mg-rich olivines experience a smaller degree of superheating and are thus ely to dissolve at a slower rate.

Kutolin & Agafonov (1978) also showed that garnet is not stable and therefore dissolves at much faster rate than olivine or pyroxene. In addition, because olivine has a higher ivation energy for dissolution than pyroxene (200 kcal mol^{-1} vs. 125 kcal mol^{-1}), it pears that the dissolution rates of olivine and pyroxene converge at greater superheatings Fig. 10).

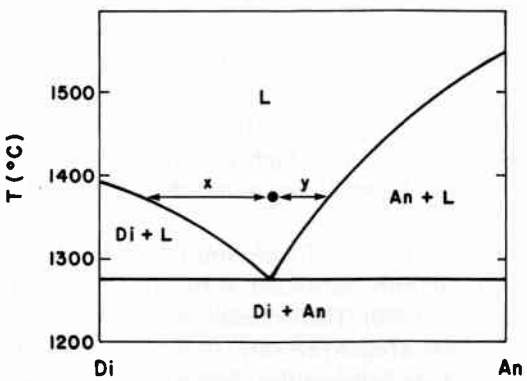

FIG. 11. The binary system diopside–anorthite used to illustrate that the relative driving forces for dissolution of anorthite (u_{An}) vs. diopside (u_{Di}) in the eutectic melt composition at 1375 °C are related to the distance between the melt composition and the respective saturation surfaces. In this case $u_{An}/u_{Di} \approx y/x$.

In a related study, Kuo & Kirkpatrick (1985) showed that the relative dissolution rates of forsterite, enstatite and diopside in a melt in the system forsterite–diopside–silica can be qualitatively explained by the relative driving forces for dissolution. This is illustrated schematically in Fig. 11. The ratio of the dissolution rates of anorthite and diopside (u_{An}/u_{Di}) in the eutectic melt composition is approximately equal to the distance y/x. This explanation cannot easily be used quantitatively in a complex natural system. However, it can be demonstrated qualitatively that the liquidus phase relationships of a complex melt govern the relative dissolution rates at least at a small degree of superheating.

Chemical diffusiv
determined by a nun
& Watson, 1983, 19
eview of diffusivitie
1986). However, on
ation diffusivities a
melt.

Chekhmir & Epel
nducted in an albi
elated to the minera
issolution rates, thu
not possible. Howe
iffusion coefficient c
rders of magnitude
ikely to be more stab
at a much slower rate
djacent to dissolving
hat there is an intim
ltimately determine
me conclusions ca
Chekhmir & Epel'ba
olecules released int
nd therefore that the
hat the dissolving mi
he diffusivity of the 'c
ot appropriate to de

The conclusion we
iffusing complex is i
he melt during a disso
tructural or surface
o diffuse away from
nanometric, the diff
he mobility of the
mplicate that cation d
ation because the
neral dissolution r
eration and multi-c
ystics which

Chemical diffusiv
etermined by a nun
k Watson, 1983, 19
eview of diffusivitie
1986). However, on
ation diffusivities a
ult.

Chekhmir & Epel
nducted in an albi
lated to the minera
solution rates, thu
s not possible. How
ffusion coefficient c
ders of magnitude
kely to be more stab
a much slower rate
djacent to dissolving
there is an intim
ltimately determine
conclusions ca
Chekhmir & Epel'ba
olecules released int
herefore that the
the dissolving mi
diffusivity of the 'c
appropriate to de
The conclusion we
ing complex is i
during a disso
ural or surface
diffuse away from
metric, the dif
mobility of the
that cation d
because the
dissolution
and multi-c
which